# OpenFOAM-based Numerical Simulation on Capillary Flow in Closed Hierarchical Microchannels

Kumar, Gaurav
Graduate School of Engineering, Kyushu Institute of Technology

Zhang, Datong
Graduate School of Engineering, Kyushu Institute of Technology

Nagayama, Gyoko
Department of Mechanical Engineering, Kyushu Institute of Technology

https://doi.org/10.5109/7157999

出版情報：Proceedings of International Exchange and Innovation Conference on Engineering & Sciences (IEICES). 9, pp.343-348, 2023-10-19. 九州大学大学院総合理工学府
バージョン：

# OpenFOAM-based Numerical Simulation on Capillary Flow in Closed Hierarchical Microchannels

Gaurav Kumar[1], Datong Zhang[1], Gyoko Nagayama[2*]
[1]Graduate School of Engineering, Kyushu Institute of Technology, Kitakyushu, Fukuoka 804-8550, Japan
[2]Department of Mechanical Engineering, Kyushu Institute of Technology, Kitakyushu, Fukuoka 804-8550, Japan
*Corresponding author email: nagayama.gyoko725@mail.kyutech.jp

**Abstract:** *Surfaces with hierarchical micro/nanoscale structures result in unique flow characteristics in nature. The validity of the classical Lucas–Washburn equation has been argued for the capillary-driven flow in open rectangular microchannels. Meanwhile, there is no guarantee that the Lucas–Washburn equation is valid for the capillary-driven flow in hierarchical microchannels. Here, we perform 3D numerical simulations using the OpenFOAM Volume-of-Fluid method to predict the capillary-driven flow of water in a closed hierarchical microchannel. It is found that the imbibition rate is increased in the hierarchical microchannel, and the mean imbibition rate shows a dependence on the height of minor channel. Consequently, an optimized hierarchical channel geometry has been proposed to improve the capillary flow in microchannels.*

**Keywords:** Capillary-driven flow; Hierarchical channel; Imbibition rate; Contact angle; OpenFOAM

## 1. INTRODUCTION

Capillary-driven flow, also known as capillary wicking is a common phenomenon observed in nature at various scales [1]. Capillary microfluidic devices are one of the major applications where no external power supply is needed to transport the fluid. The synergic interactions of capillary geometry, fluid properties, and solid-liquid interaction play an important role in deciding the imbibition of the fluid [2]. Imbibition rate in capillary-driven channels is often used for assessing system performance. Particularly, in lab-on-a-chip devices, the rapid delivery of fluid samples can accelerate the overall sample analysis. Moreover, the heat pipe needs a higher capillary mass flow rate to transport the working fluid from the condenser region to the evaporator region.

In the context of fluid transportation through microchannels, the ability to transport fluid is determined by the critical pressure, which is influenced by several factors. One of these factors is the Laplace pressure (ΔP), which depends on the interfacial tension of the fluid, the advancing contact angles (θ) between the fluid and the surrounding surfaces, as well as the dimensions of the microchannel. The contact angles of the fluid on the inner surfaces of the microchannels are determined by the interfacial forces present at the solid-liquid-gas three-phase lines. Using the Young-Laplace equation, a relationship between the interfacial tension, contact angle, and the radius of curvature of the capillary is shown in equation (1).

$$\Delta P = \frac{2\sigma \cos\theta}{r} \qquad (1)$$

where σ is the surface tension of the fluid and $r$ is the capillary radius. Consequently, any changes or modifications to the physicochemical properties of the inner surfaces of the microchannels will directly impact the original interactions between these surfaces and the transportation of liquid. Ultimately, these alterations will significantly influence the flow behaviors at the microscale. Various researchers have explored the use of microstructures with inspired by nature, to enhance the understanding of fluid behavior, improve transport efficiency, and optimize microfluidic devices [3]–[9]. Chen et al. studied water harvesting and transport in hierarchical structures found on the surface of a *Sarracenia* trichome. This exceptional water transport speed is attributed to the hierarchical microchannel organization of the trichome. They also found that the highest mass transfer rate is when the number of ribs is two [7]. Zhang et al. studied unidirectional liquid spreading in the biomimetic microcavities inspired by the peristome of *Nepenthes alata* [3]. The authors claimed that by mimicking the structure of the peristome, they obtained asymmetric liquid spreading with higher accuracy. Jafari et al. used 3D metal printing to fabricate a freeform porous structure for capillary wicking. Due to the permeability factor created due to porous structure, they were able to enhance the capillary performance [10]. It is clear from the previous works that adding nature-inspired micro-structures to the microchannel surface can alter the capillary flow performance. For hierarchical-structure geometries, the optimal dimension for fluid transport due to capillary force in microchannels remains uncertain. Studying the effect of biomimetic surfaces on capillary performance experimentally requires a costly fabrication method and the classical Lucas–Washburn equation (*as shown in equation (2)*) cannot accurately predict the flow characteristics of such channels. Whereas, numerical simulations can be used as an alternative to perform such studies. Various research using numerical simulations have proven to be used as a preliminary study which is also inexpensive and less time-consuming [11]–[14].

$$x(t) = \sqrt{\frac{\sigma D_h \cos\theta}{4\mu} t} \qquad (2)$$

where, $x(t)$ is the meniscus position varying with time $t$, $D_h$ is the hydraulic diameter of the channel, and $\mu$ is coefficient of dynamic viscosity of the fluid.

In this paper, the capillary flow performance in a closed hierarchical channel is studied using numerical

simulations. Furthermore, this study aims to find an optimal hierarchical channel geometry which can offer higher capillary imbibition rate.

## 2. NUMERICAL SIMULATION

### 2.1 Geometry of microchannel

A hierarchical microchannel with a major channel and a minor channel has been constructed as shown in Figure 1. In the present study, the geometry constitutes of a number of ribs *n*=2, as it claims to have a high flux ratio in hierarchical channels [7]. The total length of the channel is 30 mm with the height (H) and width (W) of the major channel as 100 µm and 200 µm. The width of the minor channel ($W_{minor}$) is fixed to be 100 µm, the height of the minor channel ($H_{minor}$) is varied from 2 µm ~ 50 µm, and the rib thickness δ is10 µm.

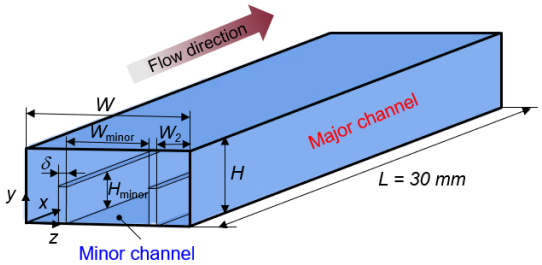


Figure 1. Geometry of the hierarchical microchannel.

### 2.2 Governing equations

Using the volume-of-fluid (VOF) method, transient, three-dimensional numerical simulations of the capillary flow in hierarchical microchannel have been performed. The system comprises two fluids, namely liquid and gas phases, which are incompressible and cannot be mixed together. The VOF method considers the influence of surface tension [15]. The specific fluids involved are water as the liquid, and air as the gas. Within this method, the momentum equation and continuity equation have been addressed. The flow is assumed to be laminar, incompressible, Newtonian, and isothermal. The velocity field V is governed by the Navier-Stokes and continuity equations, expressed as follows:

$$\nabla . V = 0 \qquad (3)$$

$$\frac{\partial \rho V}{\partial t} + \nabla . (\rho VV) = -\nabla P + \rho g + \nabla . \left(\mu(\nabla V + \nabla^T V)\right) + F_s \qquad (4)$$

In equation 2, the velocity of the mixture is represented by *V*, while *P* denotes the pressure, t indicates the time, and $F_s$ represents the volumetric force originating from surface tension at the interface. Furthermore, $\boldsymbol{\rho}$ and $\mu$ represent the density and dynamic viscosity, respectively. Within this equation, the accumulation and convective momentum terms within each control volume (cell) are responsible for maintaining a balance between the pressure force, gravity force, shear force, and the supplementary force resulting from surface tension, $F_s$.

The physical properties of each fluid are determined by calculating weighted averages based on the volume fraction of the individual fluid present in a single cell. The fluid volume within a cell is computed as $F_{vol} = FV_{cell}$, where $V_{cell}$ represents the volume of a computational cell and F denotes the liquid volume fraction within that cell. The value of F within a cell should fall between the range of 1 and 0. A value of F = 1 signifies a cell that is entirely filled with liquid, while F = 0 indicates a cell completely filled with gas. Values of F ranging from 0 to 1 represent the interface between the liquid and gas phases.

To ascertain the distribution of the liquid volume fraction, one can solve an additional passive transport equation, which is expressed as:

$$\frac{\partial F}{\partial t} + V . \nabla F = 0 \qquad (5)$$

where F is the fraction representing cell volume filled with liquid to the total volume of the control cell. Using the volume fraction function, the physical properties of the mixture is derived computationally as follows:

$$\rho = F\rho_2 + (1 - F)\rho_1 \qquad (6)$$

$$\mu = F\mu_2 + (1 - F)\mu_1 \qquad (7)$$

Here, 1 and 2 represent the gas and mixture phases, respectively.
As the capillary force mainly depends on surface forces, the surface tension is computed using the continuum surface force (CSF) model. The model equation is as follows:

$$F_s = \sigma \kappa \nabla F \qquad (8)$$

In the CSF model, the surface tension remains constant across the surface, and the forces that act perpendicular to the interface are considered. To calculate the surface curvature, denoted as κ, the following equation is used:

$$k = \frac{1}{|n|}\left(\left(\frac{n}{|n|} . \nabla\right)|n| - \nabla . |n|\right) \qquad (9)$$

Here, $\mathbf{n} = \nabla F$ is denoted as the normal vector and the contact angle θ includes the wall adhesion forces using the following relation:

$$\hat{n} = \hat{n}_w \cos\theta + \hat{t}_w \sin\theta \qquad (10)$$

To find the liquid volume fraction and velocity field solution in this study, equations (3) to (10) are solved through an iterative process. This involves considering the appropriate initial and boundary conditions. This study does not consider gravity's influence since the Bond number ($Bo = \boldsymbol{\rho} g H^2/\sigma$) is significantly lower than unity.

### 2.3 Initialization & boundary conditions

At time t = 0, the liquid meniscus is positioned 1 mm away from the inlet of the hierarchical channel. The walls of the channel are considered to have a no-slip boundary condition, and the surface affinity is determined by the contact angles. In this case, contact angle values of 30, 50, and 80 degrees are assigned to all the walls of both major and minor channels. At the inlet, a liquid volume fraction value of 1 is specified, indicating that the entire space is filled with liquid. On the other hand, at the outlet of the channel, a liquid volume fraction value of 0 is set, indicating that there is no liquid present at that location.

### 2.4 Solution method

In the present study, computational fluid dynamics (CFD) simulations were performed using a C++ library-based OpenFOAM v2012 [16]. OpenFOAM (Open Field Operation and Manipulation) is an open-source CFD software package widely used for simulating fluid flow and heat transfer phenomena in various engineering and scientific applications [14], [17]–[20]. The chosen method to solve the partial differential equations on a 3D unstructured mesh of polyhedral cells follows the finite volume approach. To accurately capture sharp fluid/fluid interfaces in the present capillary-driven flow, the solver employs the VOF (Volume of Fluid) two-phase algorithm. Since a transient solution is desired, selecting an appropriate time step is crucial for ensuring numerical stability during the simulation. In this case, a target Courant-Friedrichs-Lewy (CFL) number of 0.1 is applied to maintain stability. This means that during each time step, the interface is allowed to cross 10% of the width of a grid cell in the VOF computation. To couple pressure and velocity and perform pressure correction, the solver utilizes the Pressure Implicit with Splitting of Operators (PISO) algorithm. Additionally, to achieve the necessary compression of the interface and prevent its separation, especially in diverging flows, an artificial compression term is introduced into the VOF equation. By employing these techniques and algorithms, the solver ensures accurate and stable numerical simulations, allowing for the analysis of complex capillary-driven flows and the capturing of intricate fluid interfaces. Various parameters used in the simulation are listed in the table below:

**Table 1**. Simulation parameter values in present analysis

| Simulation Parameter | Value |
|---|---|
| Surface tension, σ | 0.0707 N/m |
| Courant number $_{maximum}$ | 0.2 |
| Scheme | *Gauss linear* |
| $\Delta t$ | 1e-5 |
| Number of mesh elements | 600,000 |

The computations are performed on high-performance computing (HPC) environment within a clustered parallel environment based on an open message passing interface (OpenMPI) library. The mesh decomposition was conducted using *decomposePar* and the domains were divided into 125 processors (number of nodes = 2).

## 3. RESULTS AND DISCUSSION

### 3.1 Model validation

Before simulating the hierarchical microchannel, it is important to validate the VOF model for capillary-driven flow with theory or experiment. To do so, a closed rectangular microchannel with no hierarchical structure has been selected. The total length of the channel is 30 mm with the height (H) and width (W) of the channel as 100 µm and 200 µm respectively. Three cases with contact angles 30, 50 and 80 degrees respectively is considered and the simulation results are compared with L-W equation. The hydraulic diameter for L-W equation is calculated as $D_h = 4A/P$, where A is the cross-section area and P is the wetted perimeter.

Figure 2(a) shows the theoretical validation of the simulation results. It can be observed that the capillary flow trend is consistent in both theory and simulation. At lower theta values such as 30° and 50°, there is a slight underprediction which is expected due to the corner flow [21], [22]. But as the theta value (hydrophobicity) increases, which is in the case of 80°, the corner flow becomes negligible and thus the theory well matches with the simulation. This can be understood by looking at the shape of the meniscus in Figure 2(b). Overall, a non-linear displacement trend for the meniscus is obtained which matches well with the literature[23], [24].

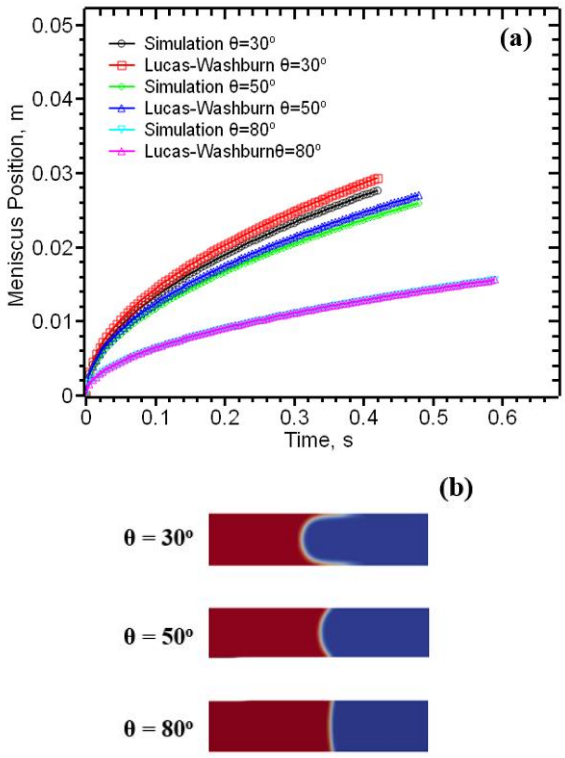


Figure 2. (a) Validation results for rectangular microchannel of different wettability with L-W equations (b) 2-D meniscus shapes for different wettability at t=0.1 seconds.

### 3.2 Capillary performance in hierarchical channel

In the present simulation, five different values for minor channel height ($H_{minor}$ = 2 µm, 5 µm, 10 µm, 25 µm, 50 µm) have been selected. The effect of minor channel height on the capillary flow can be observed by looking at the meniscus position in the hierarchical channel. Because of the two different widths ($W_{minor}$ and $W_2$) present inside the hierarchical channel with $W_{minor} > W_2$, the flow proceeds in the channel with width $W_2$ which is also a part of the major channel. Therefore, in the subsequent graphs, it can be seen that the meniscus position in the major channel is ahead of that of the minor channel. Figures 3-5 show the plot for meniscus position with respect to time. In the case of $H_{minor}$ = 2 µm, it can be seen from Figure 3 that the meniscus positions in the major and minor channels approximately overlap each other. This is mainly due to the insignificant presence of the minor channel as $H_{minor}/H$ = 0.02. Although the meniscus in major and minor channels travel together, there is an increase in the mean imbibition rate due to this structural change compared to the no hierarchical

channel as shown in Figure 6. In the case of $H_{minor}$ = 10 µm as shown in Figure 4, the meniscus position in the major channel is ahead of that in the minor channel. The difference between the positions increases with time. This is obvious because as the minor channel height increases, the capillary strength increases. Here, the presence of a minor channel is more significant as $H_{minor}/H$ = 0.1. It is also known that viscous force which is resistant to the capillary direction also increases with the increase in minor channel height. As shown in Figure 5, when the minor channel height becomes half of the major channel height (*i.e.*, $H_{minor}/H$ = 0.5), the flow in major and minor channel separates since the beginning of the flow. Due to this separation of flow in both channels, an elongated meniscus is observed. This meniscus elongation phenomenon shown in Figure 7 is caused due to the corner flow.

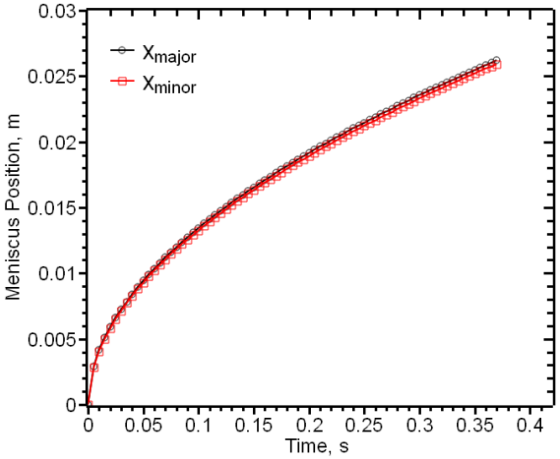


Figure 3. Transient meniscus displacement with time for hierarchical microchannel with $H_{minor}$ = 2 µm.

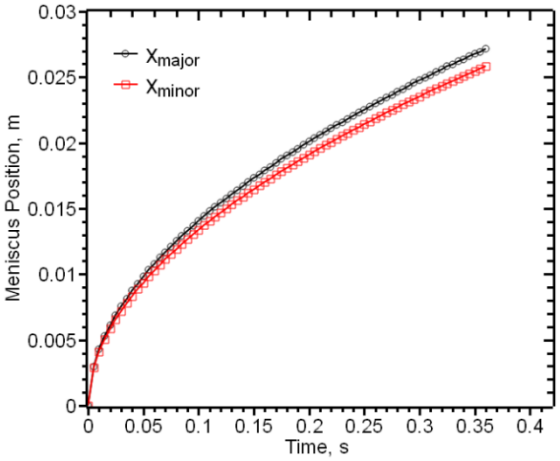


Figure 4. Transient meniscus displacement with time for hierarchical microchannel with $H_{minor}$ = 10 µm.

The capillary performance is assessed by taking the mean imbibition rates at two positions: x = 15 mm and x = 25 mm. The mean imbibition rate increases as minor channel height increases until a maxima value is reached. Then after, mean imbibition rate starts decreasing with the increase in minor channel height. Figure 6 (a) shows this trend as it can been seen that the maximum mean imbibition rate is found when $H_{minor}$ = 10 µm. At x=15 mm, the mean imbibition rate for a rectangular channel without hierarchical structure is 106.77 mm/s whereas adding hierarchical structure enhanced the mean imbibition rate to 119.89 mm/s and 113.81 mm/s in major and minor channels respectively. Similarly, at x = 25 mm, the mean imbibition rate for a rectangular channel without hierarchical structure is 68.50 mm/s whereas 76.77 mm/s and 72.88 mm/s in major and minor channels respectively.

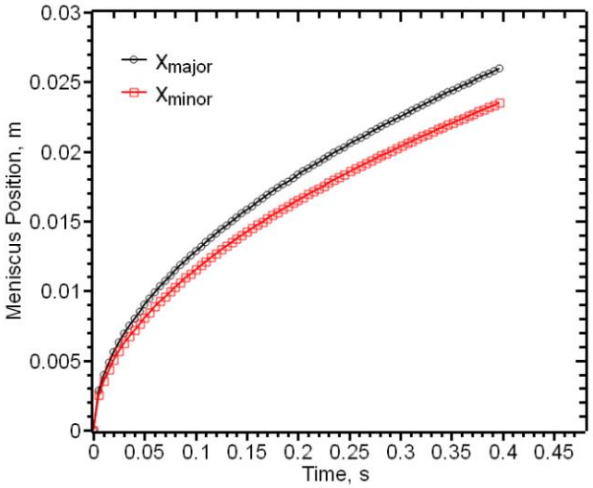


Figure 5. Transient meniscus displacement with time for hierarchical microchannel with $H_{minor}$ = 50 µm.

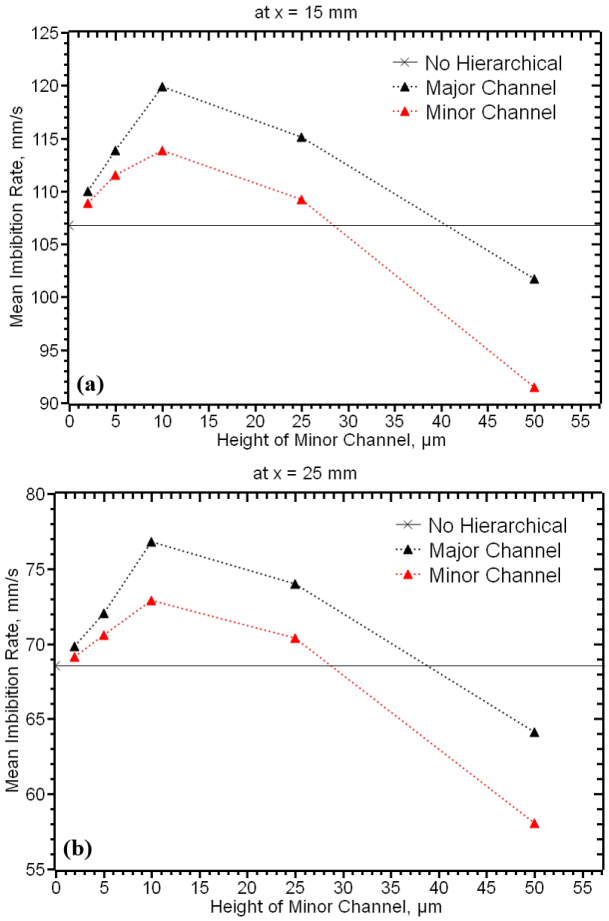


Figure 6. Variation of mean imbibition rate with minor channel height (a) at x=15 mm, (b) at x = 25 mm.

The capillary number (Ca) is a dimensionless parameter used to characterize the relative importance of viscous forces to capillary forces in fluid flow within small channels or porous media [25]. It is defined as the ratio of viscous forces to surface tension forces and is given by equation (11).

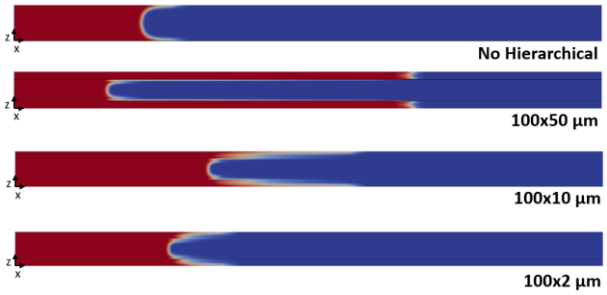


Figure 7. Comparison of elongated meniscus shape in hierarchical channel with varying minor channel height.

$$Ca = \frac{\mu U}{\sigma} \qquad (11)$$

where, $U$ is characteristic velocity of the fluid flow. To validate the capillary performance in the hierarchical channel, capillary number were calculated and compared. A similar trend to mean imbibition rate was observed.

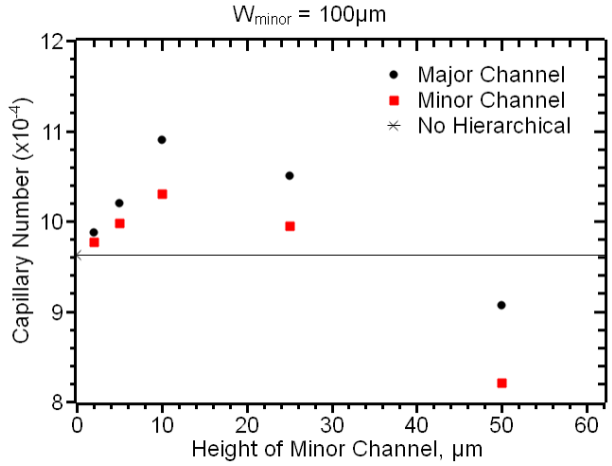


Figure 8. Capillary number for major and minor channels with varying minor channel height.

### 3.3 Wettability effect on the capillary performance

From the previous section, it became evident that by using hierarchical structure in the microchannel, capillary imbibition rate can be enhanced. Now, it is important to make sure if the hierarchical microchannel can be effective of fluids with different wettability. For this, the best performing hierarchical channel with $H_{minor}$ = 10 µm was selected and the fluid contact angle was varied. Figure 9 shows a comparison of mean imbibition rate between hierarchical and no-hierarchical channels. At lower contact angle i.e. θ = 30°, a significant difference in the mean imbibition rate between hierarchical and no-hierarchical channels is observed. Whereas when the contact angle increases, i.e. for θ = 50° or 80° there is an insignificant difference in the mean imbibition rate between hierarchical and no-hierarchical channels. When the centerline meniscus reaches at x = 15 mm, it can be seen from Figure 9 (a) that in all three cases (θ = 30°, 50° and 80°), mean imbibition rate is higher in hierarchical channel. But the difference in mean imbibition rate is almost negligible in major and minor channels for the case of θ = 50° and 80°. However, when the centerline meniscus reaches at x = 25 mm, it can be seen from Figure 9 (b) that in the case of θ = 30°, the hierarchical channel is faster; but in the case of θ = 50°, the mean imbibition rate in hierarchical channel and no-hierarchical channel is almost same. This reduction of difference in the imbibition rate at higher contact angle occurs because the corner flow diminishes. It can be seen from Figure 10 that when the contact angle is θ = 50° and θ = 80°, the meniscus in major channel and minor channel moves together as no corner flow occurs due to high surface affinity of the fluid.

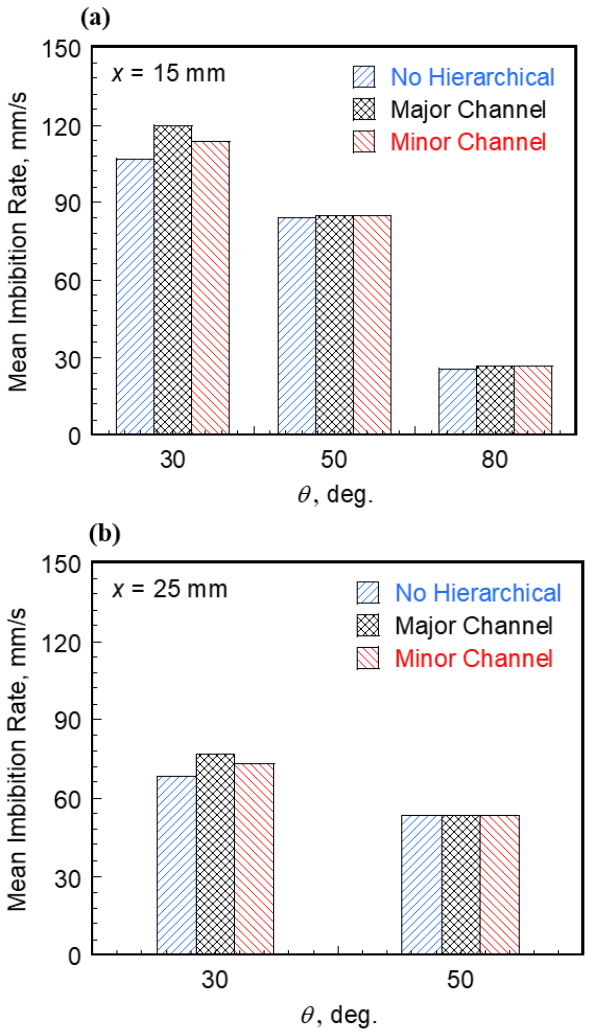


Figure 9. Comparison of mean imbibition rate (a) at x = 15 mm for θ = 30°, 50°, and 80°, (b) at x = 25 mm for θ = 30°, 50°.

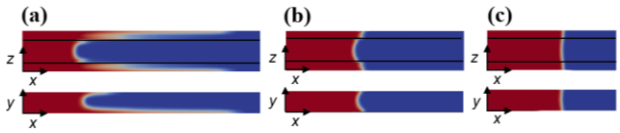


Figure 10. Comparison of meniscus shape at x = 15 mm for (a) θ = 30°, (b) θ = 50°, and (c) θ = 80°.

## 4. CONCLUSION

In this study, three-dimensional numerical simulation of capillary-driven flow in closed hierarchical microchannel with varying minor height is presented. The simulations were carried out using OpenFOAM based VOF method. The simulation results show that hierarchical microchannel can enhance the capillary imbibition rate when compared with non-hierarchical channel. If minor channel height keeps increasing, the mean imbibition rate first increases and then decreases. Therefore, an optimal hierarchical channel with $W_{minor}$ = 100 µm and $H_{minor}$ =

10 µm showed the highest imbibition rate. Corner flow plays an important role is enhancing the imbibition rate in hierarchical channel as it helps in elongating the meniscus shape. It should be also noted that hierarchical channel is more effective when fluid contact angle is more hydrophilic. The study will help in designing high performance capillary-driven microfluidic devices.

## 5. REFERENCES


[1] J. Bao and G. Nagayama, "Optimization for ultrafast capillary-driven flow in open rectangular microchannels," *International Journal of Heat and Mass Transfer*, vol. 201, Feb. 2023.

[2] A. Olanrewaju, M. Beaugrand, M. Yafia, and D. Juncker, "Capillary microfluidics in microchannels: From microfluidic networks to capillaric circuits," *Lab on a Chip*, vol. 18, no. 16. Royal Society of Chemistry, pp. 2323–2347, 21-Aug-2018.

[3] Y. Zhang, Y. Gan, L. Zhang, D. Zhang, and H. Chen, "Surface-tension-confined channel with biomimetic microstructures for unidirectional liquid spreading," *Micromachines*, vol. 11, no. 11, pp. 1–14, 2020.

[4] S. Jo, S. Ahn, H. Lee, C. M. Jung, S. Song, and D. R. Kim, "Water-repellent Hybrid Nanowire and Micro-scale Denticle Structures on Flexible Substrates of Effective Air Retention," *Scientific Reports*, vol. 8, no. 1, Dec. 2018.

[5] J. Berthier *et al.*, "Spontaneous capillary flows in piecewise varying cross section microchannels," *Sensors and Actuators, B: Chemical*, vol. 223, pp. 868–877, Feb. 2016.

[6] X. Pu, G. J. Li, and Y. H. Liu, "Progress and perspective of studies on biomimetic shark skin drag reduction," *ChemBioEng Reviews*, vol. 3, no. 1, pp. 26–40, 2016.

[7] H. Chen *et al.*, "Ultrafast water harvesting and transport in hierarchical microchannels," *Nature Materials*, vol. 17, no. 10, pp. 935–942, Oct. 2018.

[8] G. Bamorovat Abadi and M. Bahrami, "The effect of surface roughness on capillary rise in micro-grooves," *Scientific Reports*, vol. 12, no. 1, Dec. 2022.

[9] Z. Wang *et al.*, "Three-Dimensional Open Water Microchannel Transpiration Mimetics," *ACS Applied Materials and Interfaces*, vol. 14, no. 26, pp. 30435–30442, 2022.

[10] D. Jafari, W. W. Wits, and B. J. Geurts, "Metal 3D-printed wick structures for heat pipe application: Capillary performance analysis," *Applied Thermal Engineering*, vol. 143, no. July, pp. 403–414, 2018.

[11] B. Baran, K. Marzia, S. Jribi, T. Miyazaki, B. Baran Saha, and S. Koyama, "Heat and mass transfer simulation of ethanol adsorption onto activated carbon packed heat exchanger," *3 rd International Exchange and Innovation Conference on Engineering & Sciences Kyushu University, Fukuoka, Japan*, pp. 121–124, 2017.

[12] J. Ko, N. Takata, K. Thu, and T. Miyazaki, "Dynamic Simulation of a Thermal Management System Consisting of a CO_2 Heat Pump and a Water-Loop," pp. 39–43, 2019.

[13] M. Wörner, "Numerical modeling of multiphase flows in microfluidics and micro process engineering: A review of methods and applications," *Microfluidics and Nanofluidics*, vol. 12, no. 6. pp. 841–886, May-2012.

[14] A. A. Saha, S. K. Mitra, M. Tweedie, S. Roy, and J. McLaughlin, "Experimental and numerical investigation of capillary flow in SU8 and PDMS microchannels with integrated pillars," *Microfluidics and Nanofluidics*, vol. 7, no. 4, pp. 451–465, 2009.

[15] B. a. Nichita, I. Zun, and J. R. Thome, "A VOF method coupled with a dynamic contact angle model for simulation of two-phase flows with partial wetting," *7th International Conference on Multiphase Flow*, pp. 1–8, 2010.

[16] H. G. Weller, G. Tabor, H. Jasak, and C. Fureby, "A tensorial approach to computational continuum mechanics using object-oriented techniques," *Computer in Physics*, vol. 12, no. 6, pp. 620–631, Nov. 1998.

[17] S. Pavuluri, J. Maes, and F. Doster, "Spontaneous imbibition in a microchannel: analytical solution and assessment of volume of fluid formulations," *Microfluidics and Nanofluidics*, vol. 22, no. 8, pp. 1–18, 2018.

[18] L. Yang, A. Ładosz, and K. F. Jensen, "Analysis and simulation of multiphase hydrodynamics in capillary microseparators," *Lab on a Chip*, vol. 19, no. 4, pp. 706–715, 2019.

[19] M. Gholizadeh Ansari, "Numerical modeling of capillary-driven flow in open Numerical modeling of capillary-driven flow in open microchannels: An implication of optimized wicking fabric design microchannels: An implication of optimized wicking fabric design."

[20] D. A. Hoang, V. Van Steijn, L. M. Portela, M. T. Kreutzer, and C. R. Kleijn, "Modeling of low-capillary number segmented flows in microchannels using OpenFOAM," in *AIP Conference Proceedings*, 2012, vol. 1479, no. 1, pp. 86–89.

[21] N. Kubochkin and T. Gambaryan-Roisman, "Capillary-driven flow in corner geometries," *Current Opinion in Colloid and Interface Science*, vol. 59. Elsevier Ltd, 01-Jun-2022.

[22] B. Ma, "Analysis of Capillary Flow in a Parallel Microchannel-Based Wick Structure with Circular and Noncircular Geometries," *Langmuir*, vol. 36, no. 45, pp. 13485–13497, Nov. 2020.

[23] B. M. Mognetti and J. M. Yeomans, "Capillary filling in microchannels patterned by posts," *Physical Review E - Statistical, Nonlinear, and Soft Matter Physics*, vol. 80, no. 5, Nov. 2009.

[24] É. Ruiz-Gutiérrez *et al.*, "The long cross-over dynamics of capillary imbibition," *Journal of Fluid Mechanics*, vol. 939, May 2022.

[25] K. Fallah and E. Fattahi, "Splitting of droplet with different sizes inside a symmetric T-junction microchannel using an electric field," *Scientific Reports*, vol. 12, no. 1, pp. 1–12, 2022.